Materials Chemistry and Physics 199 (2017) 557–566

Contents lists available at ScienceDirect

Materials Chemistry and Physics

journal homepage: www.elsevier.com/locate/matchemphys

Bio-prototyping of europium-yttria based rods for radiation dosimetry

S.C. Santos*, O. Rodrigues Jr., L.L. Campos

Instituto de Pesquisas Energeticas e Nucleares – IPEN, Av. Prof. Lineu Prestes 2242, Cidade Universitaria, Sao Paulo, Brazil

HIGHLIGHTS

- Alternative hydrothermal synthesis of powders is demonstrated.
- Bio-prototyping of europium-yttria rods is reported.
- Microstructure evolution of as sintered rods is evaluated.
- The effect of Eu^{3+} on paramagnetic response of yttria host is discussed.

GRAPHICAL ABSTRACT

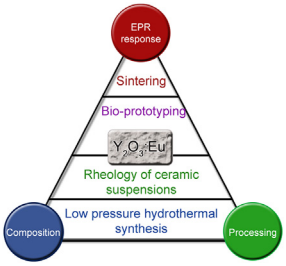

ARTICLE INFO

Article history:
Received 28 March 2017
Received in revised form
26 June 2017
Accepted 15 July 2017
Available online 17 July 2017

Keywords:
Yttria
Rare earths
Radiation dosimetry
Bio-prototyping
Ceramic processing

ABSTRACT

The application of solid state dosimeters in radiation protection has grown significantly as consequence of advances in the development of dosimetric materials using rare earths. The conception of new dosimetric materials concerns synthesis methods, which control the evolution of material structure, including further processing steps as, shaping, drying, and sintering. The present study reports a full bio-prototyping approach to produce europium doped yttria rods with potential application in radiation dosimetry. Ceramic particles synthesized by hydrothermal route were characterized by Photon Correlation Spectroscopy (PCS), X-ray diffraction (XRD), and Scanning Electron Microscopy (SEM). The effect of europium on promoting electronic defects in yttria host was evaluated by Electron Paramagnetic Resonance (EPR). Low pressure hydrothermal synthesis led to formation of rounded particles with mean diameter of 410 nm. Aqueous suspensions with 20 vol% of particles prepared at pH 10, and 0.2 wt% binder exhibited apparent viscosity of 213 mPa s, being suitable for bio-prototyping of rods. Sintering of shaped samples at 1600°C for 4 h provided formation of dense ceramic rods. Europium-yttria rods containing 5 at.% Eu exhibited the most intense EPR response.

1. Introduction

A basic feature of dosimeter material is the ability to absorb radiation energy and release it in form of visible light as photon or thermally stimulated. The mechanism that converts absorbed radiation energy into visible light output depends on material characteristics such as chemical composition and crystal structure. Besides, these characteristics are consequence of synthesis route, including the nature of starting materials and further processing steps.

The structure of material, including its defects (intrinsic and extrinsic) can be controlled by synthesis methods such as evaporation [1], Pechini [2], chemical vapour deposition (CVD) [3], spray pyrolysis [4], sol-gel [5], co-precipitation [6], hydrothermal [7], and combined synthesis methods [8]. Usually these routes lead to formation of powder materials, in which further processing steps are required to produce the desired product. Recently our group presented a facile hydrothermal synthesis using environmental

* Corresponding author.
E-mail address: silas.cardoso@alumni.usp.br (S.C. Santos).

http://dx.doi.org/10.1016/j.matchemphys.2017.07.063
0254-0584/

pressure and temperature around of 60 °C to obtain submicrometer yttrium disilicate powders, with mono modal particle size distribution, rounded shape, high specific surface area and pycnometric density similar to theoretical one [9,10].

Nowadays our research group has reported approaches on development of advanced materials by bio-prototyping using renewable materials [9,11–15]. Yttria nettings with homogeneous void shape were produced using wood based netting as template [12]. Biomorphic burners with thermoluminescence response based on dysprosium doped yttrium disilicate were formed from Luffa Cylindrica vegetable sponge [14]. Yttria micro rods with dense microstructure and electron paramagnetic response were shaped from wheat starch templates [11].

Bella et al. [16–18] employed carboxymethyl cellulose (CMC) and micro fibrillated cellulose (MFC) as bio-sourced materials to produce quasi-solid electrolytes for polymeric dye-sensitized solar cells (DSSCs). Nishiyama et al. [19] using alginate hydrogel and inkjet printing produced 3D biological structures composed of living cells in vitro, which procedure was termed as 3D printer. Zolin et al. [20] proposed a new solid Li-ion cell structural design based for LiFePO4/graphite electrodes using carbonised cellulose nanofibrils.

Colloidal processing consists in a full procedure to obtain advanced materials since manipulation of molecular structures (colloids), including the control of inter-particle forces, followed by consolidation of colloidal particles into a desired shape and finally, the enhancement of interparticle bonds by means of thermal treatment. Recently our research group has published some contributions addressing colloidal processing and bio-prototyping of rare earth ceramics such as, yttria nettings [12]; bio-prototyping rare earth doped yttria ceramics [15], yttrium disilicate microcellular ceramics [9] and, biomorphic dysprosium doped yttrium disilicate burners [14].

Yttria (Y_2O_3) is a promising material for radiation dosimetry due to its intrinsic chemical and physical proprieties as melting point of 2400 °C, refractive index of 1.9, thermal and chemical stability. Besides, Y_2O_3 is used for enhancement of sintering [21], catalysis [22], luminescence [23], electrical [24], electronic [25], mechanical [26] and thermal [27] behavior of many advanced materials. Europium doped yttrium oxide (Y_2O_3:Eu^{3+}) is noted for its excellence in luminescence [28]. ZHANG et al. [29] reported the synthesis of single-layer yttrium oxide nanosheets doped with Eu^{3+} and Tb^{3+} by the exfoliation method. As synthesized nano sheets exhibited transparency, strong red and green emissions, these results rise it as potential to be used as building blocks and other functional materials.

Considering yttria potential for radiation dosimetry and our experience on processing of rare earth powders, this work reports a full colloidal processing of europium doped yttria rods as following: stoichiometric composition of material, powders synthesis, rheology of suspensions, bio-template evaluation, bio-prototyping, microstructural evolution of rods as a function of sintering parameters, and effect of europium on EPR response of yttria rods.

2. Experimental

For development of europium-yttria powders (Y_2O_3:Eu) with controlled size, shape and stoichiometry the following starting materials were used: yttria (Y_2O_3, 99.99%, Alfa Aesar GmbH), europium oxide (Eu_2O_3, 99.999%, Alfa Aesar GmbH), nitric acid (HNO_3, Synth), ammonium hydroxide (NH_4OH, Casa Americana).

Synthesis of Y_2O_3:Eu powders with up to 10 at%. Eu^{3+} was performed by a facile hydrothermal process, based on environmental pressure and temperature of 60 °C. Aqueous solutions of yttrium nitrate ($Y(NO_3)_3 \cdot 6H_2O$) and europium nitrate ($Eu(NO_3)_3 \cdot 6H_2O$) were prepared by dissolution of rare earth powders in HNO_3. Considering the stoichiometry of final powders, aqueous solutions based on yttrium and europium nitrates were stirred together, followed by addition of NH_4OH to adjust pH of final solution. The precursor gel suspension was formed at pH 10, corresponding to europium-yttrium hydroxide (Eq. (1)). The present gel was stirred at 60 °C for 6 h, using a condenser system to maintain constant the volume of suspension.

$$(2-a)Y(NO_3)_{3(aq)} + (a)Eu(NO_3)_{3(aq)} + NH_4OH_{(aq)} \xrightarrow{60^{\circ}C} Y_{(2-a)}Eu_a(OH)_{3(s)} + 3NH_4(NO_3)_{(aq)} \quad (1)$$

The precursor gel was dried at 70 °C for 24 h, followed by thermal treatment up to 1200 °C in air atmosphere using a box furnace (Lindberg Blue, Haake) as shown in Fig. 1. Thermal treatment of precursor powders (YE) was based on thermal decomposition assay of powders. A sample of 10 mg was heating up to 1400 °C in air atmosphere (Lindberg Blue, Haake), in which its mass was measured in each 100 °C, using an analytical balance (Mettler Toledo, AB204-S). The first derivate of mass loss curve as a function of temperature was calculated in order to determine in which temperature the maximum decomposition peak of sample takes place.

Powder characterization consisted in determining the mean particle size (d_{50}) by means of Photon Correlation Spectroscopy (PCS, ZetaPALS Analyzer, Brookhaven Instruments) and using hydrodynamic diameter model [30] as shown in (Eq. (2)); X-ray diffraction (XRD, Rigaku Multiflex, Japan), with an angular range (2θ) from 15 to 70°, scanning of 0.5°.min^{-1} and Kα source, in which crystallite size was calculate from Scherrer formula [31] (Eq. (3)), and based on the measurement of full-width at half-maximum (FWHM) values in the corresponding XRD pattern; helium pycnometric (Pycnometer Micrometrics 1330), and Scanning Electron Microscopy (SEM, INCAx-act, Oxford Instruments).

$$d_{50} = \left(\frac{K_{BT}}{3\pi\eta(T)D_t}\right) [\text{nm}] \quad (2)$$

Where, K_{BT} is Boltzmann constant ($1.38064852.10^{-23}$ m^2. kg S^{-2}. K^{-1}), T is temperature (K), η(T) is viscosity of the suspending liquid and, D_t is particle diffusion coefficient.

$$d_c = \left(\frac{0.9\lambda}{\beta cos\theta}\right) [\text{nm}] \quad (3)$$

Suspensions with 20 vol% Y_2O_3:Eu content were prepared at pH 10 from tetramethylammonium hydroxide (TMAH, 30 wt%, Sigma Aldrich), 0.2 wt% corn starch as binder (CS, Maizena), and followed by homogenization in a ball mill for 24 h using alumina spheres ($Ø_{spheres}$ of 10 mm).

Rheological characterization of Y_2O_3:Eu suspensions was performed with a rheometer (Haake RS600, Thermo Scientific). The sensor system consists in a double-cone rotor and a stationary plate (DC60/1°). The flow behavior of the suspensions was characterized in the control rate mode (CR) and compared with rheological models available in rheometer database (Haake Rheowin Data Manager v. 3.61.0.1). All measurements were evaluated at 25° by increasing the shear rate ($\dot{\gamma}$) from 0 to 1000 s^{-1} in 5 min, holding for 2 min at 1000 s^{-1} and returning to 0s^{-1} in 5 min. For each CR step 200 points were measured.

Organic tubes based on wheat starch were used as biotemplates (BM) for replica method. BMs are abundant, renewable, low cost, and exhibit suitable inner void shape, in which filling with suspension (casting) lead to the formation of ceramic rods as shown in Fig. 1. Shape and microstructure features of BMs were

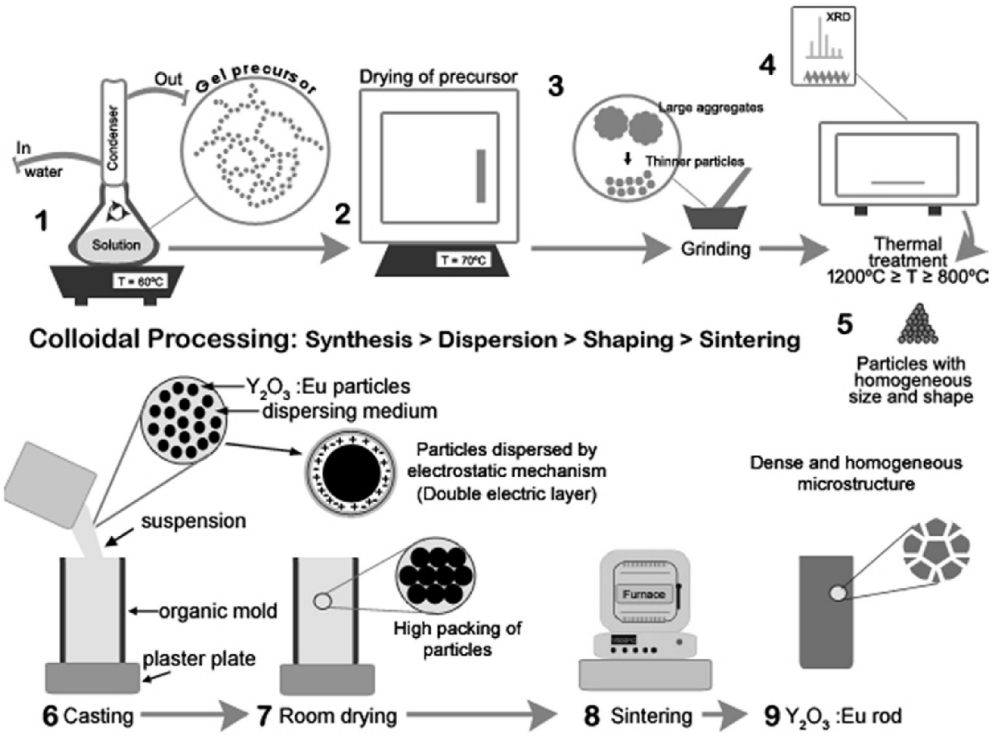

Fig. 1. Colloidal processing of Y_2O_3:Eu rods performed in this study.

observed by SEM (TM3000 Hitachi).

Thermal decomposition assay of BMs was performed by means of measuring residual mass of BMs as a function of temperature. A BM sample of 20 mg was heating up to 1200 °C in air atmosphere (Lindberg Blue, Haake), in which its mass was measured in each step of 100 °C using an analytical balance (Mettler Toledo, AB204-S). The first derivate calculation of residual mass as a function of temperature was performed in order to determine the temperature peak of maximum decomposition of sample.

Molecular composition of BMs was evaluated by Fourier transform infrared spectroscopy (FTIR, Thermo Nicolet iS50), followed by determination of the index of crystallinity (CI_{FTIR}) using Nelson et al. [32] model as shown in Eq. (4). As shaped samples were sintered in a vertical furnace (Lindberg/Blue M), in which thermal treatment conditions were based on thermal decomposition results of BMs.

$$CI_{FTIR} = \left(\frac{a_{1372}}{a_{2900}}\right) [\text{a.u.}] \quad (4)$$

where, a_{1372} and a_{2900} are the absorbance intensities of the bands at 1372 and 2900 cm^{-1} for O–H bending and C–H stretching in FT- IR spectra respectively.

Characterization of Y_2O_3:Eu rods was performed by SEM (TM 3000, Hitachi; INCAx-act, Oxford Instruments); XRD (Rigaku Multiflex), with scanning at 0.5° min^{-1}, from 15 to 70° (2Θ), Cu-Kα radiation, helium pycnometric (Pycnometer Micrometrics 1330).

Paramagnetic response of Y_2O_3:Eu rods as a function of dopant concentration (Eu^{3+}) was evaluated by electron paramagnetic resonance using a X-band EPR spectrometer (Bruker EMX PLUS), in room temperature and atmosphere. EPR spectra of samples were recorded in field modulation frequency of 100 kHz, microwave power of 2.5 mW, centre field of 300 mT, sweep width of 300 mT, modulation amplitude of 0.4 mT, time constant of 0.01 ms, 10 scans, temperature of 20 °C, environmental atmosphere, and under controlled humidity.

3. Results and discussion

Yttria exhibits crystal features that enable inserting of rare erth ions RE such as (Eu^{3+}, Tb^{3+}, Yb^{3+}, Er^{3+}) into its structure. This inserting is known as doping and its aim concerns to intensity yttria characteristics as luminescence and paramagnetism. Recent studies [33–38] have shown that Y_2O_3 is an excellent material for doping with europium, once that Y_2O_3 and Eu_2O_3 exhibits similar crystal lattice and ionic radious ($r_Y = 0.092$ nm [39]; $r_{Eu} = 0.098$ nm [40]). Doping Y_2O_3 with Eu^{3+} gives rise to substitution of Y^{3+} to Eu^{3+} in C_2 and S_6 sites with no significant distortion of crystal lattice, which means a controlled doping. Nevertheless, no studies on colloidal processing of europium doped yttria to produce promising shaped materials for dosimetry have been reported up to now.

Thermal decomposition essay of YE up to 1400 °C in environmental atmosphere is shown in Fig. 2. Bold curve represents mass variation as a function of temperature and time, in which four distinct events were observed. The first one is observed from 25 to 150 °C, which is due to broken down of weak bonded water molecules (hydration), and resulting in residual mass around of 5%. The second event takes place in temperature range between 150 and 300 °C as a result of breaking strong bonded water molecules (dehydration) and residual mass of 9%. The third event occurs from 300 to 800 °C, in which the residual mass was around 3% and may be indicative of crystallization of C-type phase of yttria. Based on these conditions, the total mass loss was 36%.

The narrow curve represents the first derivate of residual mass as a function of temperature and time (Fig. 2). The present curve illustrates the temperature in which maximum decomposition of a substance takes place. For YE the peak of maximum decomposition of europium doped yttrium nitrate takes place at 450 °C with residual mass of 20%. According to results (Fig. 1), to produce crystalline europium doped yttrium powders the following conditions

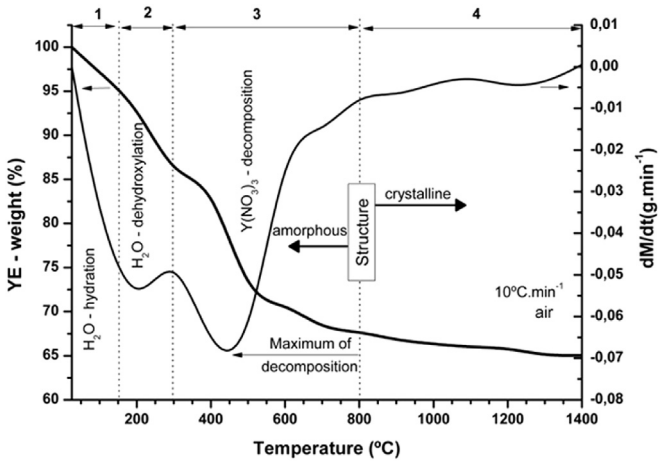

Fig. 2. Thermal decomposition of precursor powders YE evaluated up to 1400 °C in room atmosphere.

of thermal treatment were proposed: heating rate of 10 °C.min-1, step of 2 h and temperatures from 800 to 1100 °C.

XRD patterns of YE precursor powders thermally treated up to 1200 °C is illustrated in Fig. 3a. As synthesized YE powders exhibit amorphous characteristic with short range peak around of 30° (2θ). For samples under thermal treatment from 800 °C it is seen the formation of cubic C-type lattice, in which four high intensity peaks around 30.0° (222); 33.9° (400); 48.6° (440) e 57.6° (622) are presented, corresponding to Powder Diffraction File (PDF. 25–101).

Thermal treatment under 800 °C for 2 h supplied formation of cubic C-type europium doped yttria powders for compositions up to 10 at.% Eu as shown in Fig. 3b. Europium content up to 5 at.% exhibited no alteration in crystalline structure of yttria, neither diffraction peaks corresponding to secondary phases. Based on phase diagram of the system Y_2O_3-Eu_2O_3 (Fig. 4b) cubic C-type is the most stable phase, being stable up to high temperatures around 2300 °C in which Eu content is up to 40mol.%. However, the sample which composition is 10 at.% Eu a secondary phase peak was recorded at 44.5°, corresponding to Eu_2O_3 structure. This peak may be ascribed to synthesis processing, in which homogenizing (digestion) of precursor gel may not be completed.

Even though doping Y_2O_3 with 10 at.% Eu led to formation of a peak of secondary phase, the hydrothermal synthesis based on environmental pressure was able to produce crystalline rare earth powders using low temperature (60 °C). Tolstikova et al. [41] using a modified Pechini method followed by thermal treatment carried out at 1000°C within 2 h produced Y_2O_3:Nd powders with diameter of 100 nm. Lojpur et al. [42] produced nanocrystalline Y_2O_3:Yb, Er powders via self-propagating room-temperature reaction (SPRT), followed by thermal treatment up to 1100 °C within 1 h. Englade-Franklin et al. [43] via surface-directed synthesis followed by thermal treatment in two steps, 300 °C for 3 h and 800 °C for 8 h obtained Y_2O_3:Er nanoparticles with low agglomeration state.

Yttria exhibits cubic C-type structure, in which Y^{3+} ions located at symmetry point groups C_2 and C_{3ie} are surrounded by six oxygen atoms as shown in Fig. 4a. Since Eu^{3+} ion presents ionic radius size similar to Y^{3+} ion, doping yttria with europium is characterized as substitutional insertion. Eu^{3+} ions tend to occupy C_2 and C_{3i} symmetry positions to form new energy levels, as shown in Fig. 3a. Ranson et al. [44] reported that luminescence response of yttria is associated to crystallographic axis in which RE ion is situated. As RE ions are located at C_{3i}, S_6 symmetry axis low luminescence response occurs due to less probability of electronic transitions. On

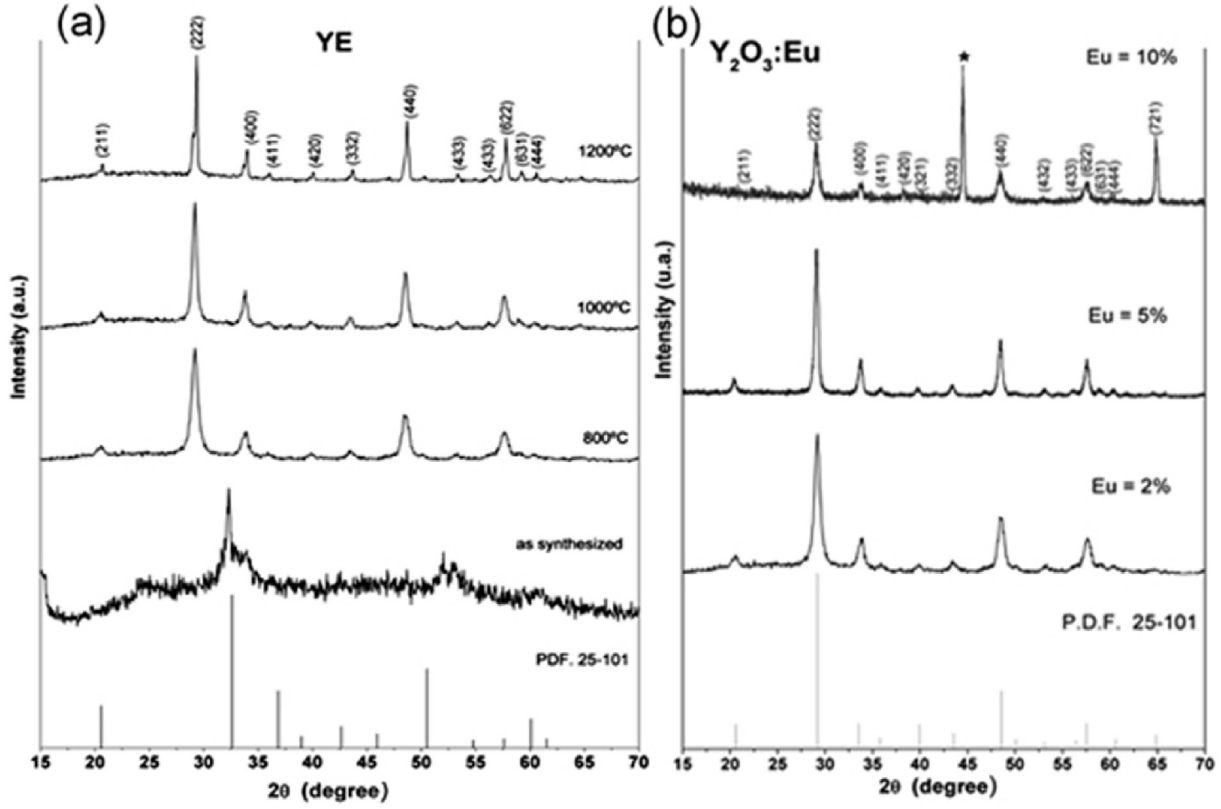

Fig. 3. XRD curves of (a) YE powders up to 1200 °C and (b) Y_2O_3:Eu powders as a function of Eu content.

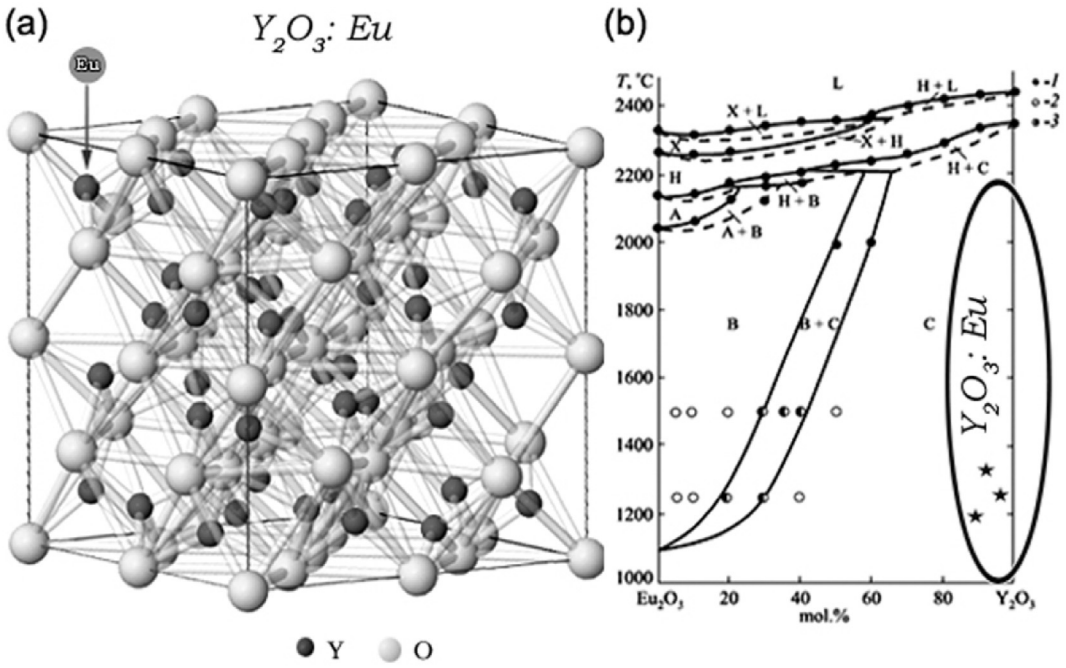

Fig. 4. Designing of Y_2O_3:Eu compositions. In (a) spheres model illustrating cubic C-type structure of yttria, in which Eu dopant can be inserted and; (b) phase diagram of Y_2O_3-Eu_2O_3 system showing all possible crystal structures as a function of dopant concentration and temperature.

the other hand, RE ions located at C_2 axis exhibit electronic transitions ($^5D0 \rightarrow {}^7F_2$) which provide higher luminescence response.

Homogeneity fields, including invariant points vary based on RE characteristics as cation size and structure. Doping Y_2O_3 with light RE (La, Ce, Pr, Nd, Y) promotes formation of solid solutions based on B type, whereas doping with middle RE (Sm, Eu, Gd, Tb, Dy) and heavy RE (Ho, Er, Tm,Yb, Lu) enable the formation of C-type in a wide range of temperature [45].

The conditions to obtain crystalline yttria based powders depend on characteristics of starting materials, synthesis route and thermal treatment parameters. Zhang et al. [46] produced europium doped yttria micro particles from hydrothermal method using autoclave, followed by thermal treatment of precursor powders at 800 °C for 5 h. Shivaramu et al. [47] synthesized yttria nanoparticles by combustion route and thermal treatment of precursor at 800 °C for 2 h. Lojpur et al. [42] synthesized terbium-erbium doped yttria particles with acicular shape by powder mixture and thermal treatment at 1100 °C for 1 h.

According to results from thermal treatment essays it is seem that the following condition of 800 °C for 2 h in air atmosphere led to formation of europium doped yttria powders with cubic C-type structure and no secondary phase peaks. The proposed hydrothermal method based on environmental pressure and temperature around 60 °C was effective in promoting the insertion of Eu^{3+} ions into yttria lattice (doping).

Fig. 5 illustrates Y_2O_3:Eu powder characteristics as a function of Eu content. Fig. 5a shows (from a_0 to a_{10} in which the subscribed number is related to dopant concentration, at.%) that increasing dopant concentration led to modification of size, shape and agglomeration state of ceramic particles. “Pure” yttria exhibits flaked particles with size around of 410 nm, whereas those doped with Eu showed rounded shape, mean diameter at least of 430 nm, and higher agglomeration state. As shown in Fig. 5b, all compositions exhibited mean particle diameter (d_{50}) and crystallite size (d_c) less than 500 nm and 11 nm respectively. In addition, increasing Eu content provided increase in pycnometric density of powders from

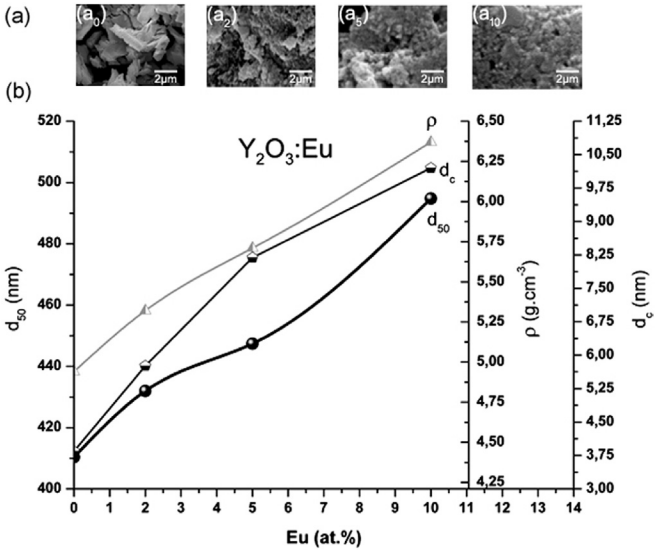

Fig. 5. Powder characterization curves of Y_2O_3:Eu as a function of Eu content.

5 to around 6.40 g cm^{-3}. According to results, it is observed that the increase of d_{50} from 410 to 490 nm is ascribed to agglomeration state of particles. Besides, variation of d_c from 3.75 to 10 nm indicates that the lattice parameters were expanded as a consequence of Eu ionic radius ($r_{Eu} = 0.098$ nm, $r_Y = 0.092$ nm) and content.

Zhao et al. [48] reported a hydrothermal method using potassium sodium tartrate ($C_4H_4O_6KNa$) as forming agent in which Y_2O_3:Eu particles with flower-like shape were obtained. According to authors, forming agent concentration leads to control nucleation and grain growth of colloidal particles and, as a consequence influences the morphology of the as synthesized particles.

Bio-template BM fits accordingly to green technology seeing

that it is based on amide starch, low cost, abundant and, as a consequence renewable. As shown in Fig. 6a, BM exhibits external diameter around of 5.9 mm, inner diameter around of 3.4 mm, and wall width around of 1.0 mm. Further, BM presents porous microstructure with grain size higher than 10 μm. BM's shape is suitable for producing ceramic rods by replica method due to its inner diameter. BM is basically constituted by organic substances, as shown in Fig. 6b. From F-TIR curve are shown vibrational peaks of C–H bonds at 2750 cm^{-1}, O–H bonds from 2400 to 1330 cm^{-1}, C–O/O–C–O stretching bonds from 1410 to 550 cm^{-1}. In addition, the index of crystallinity (CI_{FTIR}) of BM, considering the absorbance intensities of the bands at 1372 and 2900 cm^{-1} was around of 1370 cm^{-1}.

Based on our previous studies [9,12,14], it is seem that the use of starch based binders, such as corn binder (AM) leads to formation of shear thinning suspensions with apparent viscosity suitable for replica method. Fig. 5a illustrates flow curves of Y_2O_3 suspensions prepared with 20 vol% and 0.4 wt% AM in controlled rate mode. Suspensions with no AM usually exhibit constant apparent viscosity for all shear rate range evaluated and flow behavior characteristic of Carreau Yasuda model [49]. As a consequence, low viscous suspensions are not suitable for replica method, since they leak out from organic template during casting. Besides, cracks are formed as drying stage.

Ceramic suspensions based on 0.4 wt% AM (Fig. 7a) exhibited a small area between up and down curves, which is characteristic of thixotropic behavior [50]. Thixotropy consists in variation of apparent viscosity as a function of time at constant shear rate, which means that viscosity decreases due to break down of agglomerates of particles formed by long chains of AM binder. Besides, it is observed that apparent viscosity decreased while shearing, revealing flow viscous behavior. In this case, the suspension exhibits lower apparent viscosity while flowing, whereas its viscosity is higher in static mode. Shear thinning suspensions are suitable for applications as painting, pumping, impregnation, and replica. Using 0.4 wt% AM was useful to shape uniformly biotemplates, in which suspensions did not leak out from biotemplate, and the integrity of template was maintained (Fig. 7b). Therefore, 0.4 wt% AM was suitable to produce yttria rods by replica.

Processing parameters for Y_2O_3 aqueous suspensions with 20 vol% of particles and 0.4 wt% AM are described in Table 1. Based on our previous studies [9,11,12,14], it is observed that processing

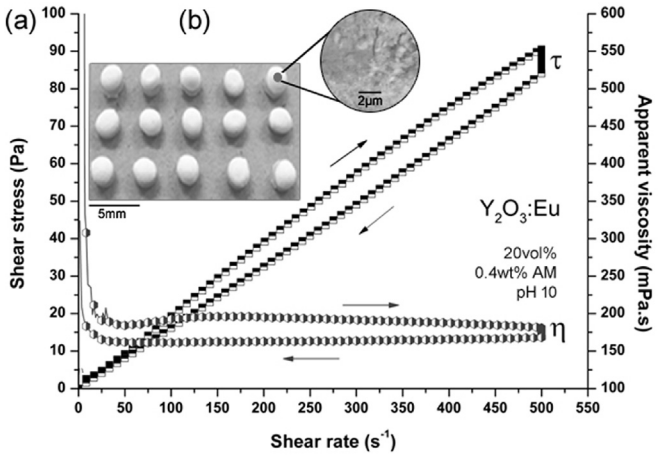

Fig. 7. In (a) Flow curves of Y_2O_3:Eu suspensions with 20 vol% of particles, pH 10 and 0.2 wt% AM and; (b) as shaped samples by replica using this suspension.

parameters change according to template characteristics. Dysprosium doped yttria nettings were produced from ceramic suspensions with 30 vol% of particles and 0.2 wt% binder. On the other hand, reticulated ceramic bulbs based on dysprosium doped yttrium disilicate were produced from ceramic suspensions containing 25 vol% of particles and 0.4 wt% binder. Therefore, to produce successfully ceramic bodies from replica method, which includes bio-prototyping, it is essential to set the condition of suspension stability as well as its viscosity considering template characteristics.

Fig. 8 shows thermal decomposition curves of BM template evaluated up to 1400 °C, with heating rate of 10 °C.min^{-1} in room atmosphere. According to mass loss curve as a function of temperature (bold curve), it is seen that BM exhibited mass loss of 10 wt% up to 175 °C due to water elimination. Accentuated degradation around 86 wt% was observed in the range of temperature between 250 and 575 °C, which corresponds to decomposition of main substances such as amylose and amylopectin. Maximum peak of decomposition (sharp curve) was recorded at 280 °C, corresponding to a mass loss of 68 wt%. In the temperature range from 575 to 1200 °C a slight variation of curve less than 1 wt% (bold curve) was observed due to decomposition of α(1,4) glucose, C-6 and, P_2O_5 units. Apart from this range of temperature, none mass variation was observed.

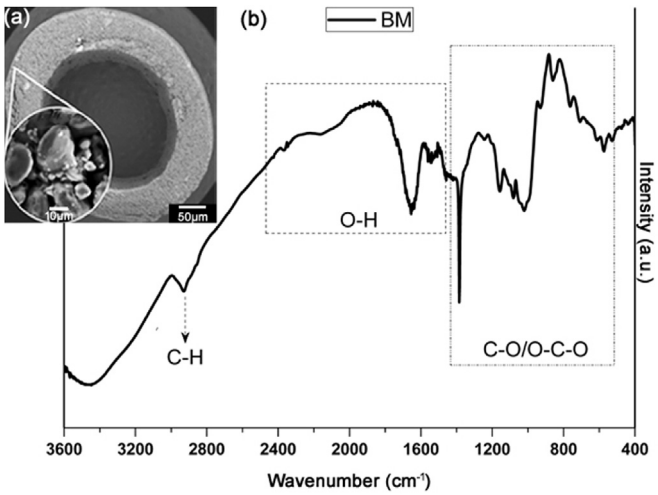

Fig. 6. FTIR spectra of BM template as received.

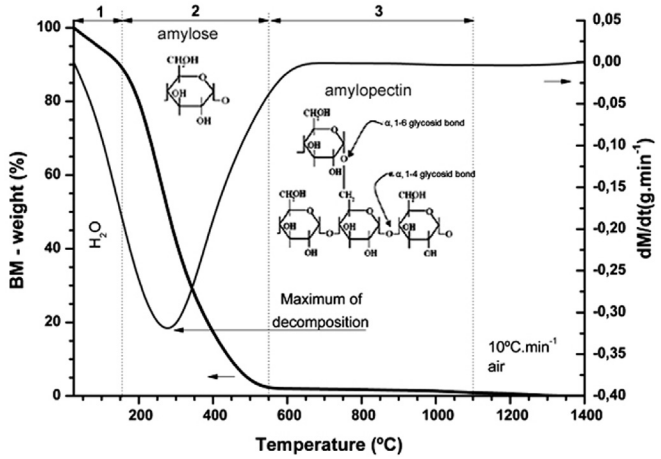

Fig. 8. Thermal decomposition curves of BM up to 1400 °C in air.

Table 1
Processing parameters of Y_2O_3 suspensions for replica method from bio-templates.

Solids (vol%)		20	
Binder (wt.%)		0.4	
η (mPa.s)		213.0	
Thixotropy (Pa.s^{-1})		$3.118.10^6$	
Rheological model	Cross	Parameters	
		η_0 (mPa.s)	2.250
		η_∞ (mPa.s)	17.25
		$\dot{\gamma}$ (s^{-1})	$1.976.10^4$
		n	0.6565

η: apparent viscosity at 10s^{-1}; η_∞: infinity viscosity; $\dot{\gamma}$: shear rate; n: power law index.

Table 2
Results of thermal treatment essays of as shaped yttria samples.

Condition	Heating rate (°C.min^{-1})	Temperature (°C)	Hold (h)	Result
1	5		2	Fragmented
2	5		4	Brittle
3	5	1600	6	Brittle
4	3		4	Strong
5	3		6	Strong

Considering thermal decomposition results of BM samples thermal treatment conditions for sintering of shaped samples were proposed as shown in Table 2. Essays from 1 to 3 were not enough to produce ceramic rods with mechanical strength and smooth shape. This condition was defined by controlling thermal decomposition of BM template while shaping and sintering of ceramic phase. The first condition led to formation of fragmented samples, whereas conditions 2 and 3 provided brittle samples. Conditions 4 and 5 provided samples with mechanical strength.

Considering results from Table 2 conditions 4 and 5 are suitable to produce europium-yttria rods by bio-prototyping. Among these conditions, condition 4 supplied samples with higher density and mechanical strength. Fig. 9 shows samples sintered on condition 4, with homogeneous size and shape (mean height, h_m of 3.335 mm ± 0.011 mm; mean diameter, $Ø_m$ of 2.271 mm ± 0.014; mean weight, m_w of 63.730 mg ± 0.002 mg), dense surface microstructure (Fig. 8c_1), and inner microstructure with cleavage planes exhibiting transgranular characteristics (Fig. 8c_2). Therefore, condition 4 was used to thermal treatment of yttria based samples by bio-prototyping.

Correlation between pycnometric density and microstructure of as sintered samples as a function of thermal treatment is shown in Fig. 10. Thermal treatment conditions from 1 up to 3 provided samples with porous microstructure and as a consequence, density inferior of 90%. On the other hand, conditions 4 and 5 supplied samples with higher density (>98% of theoretical density), heterogeneous grain shape and size higher than 2 μm.

Sintering of Y_2O_3:Eu rods (up to 10 at.%) based on condition 4 led to formation of ceramic rods with controlled shape and size, including high crystallinity as shown in Fig. 11. Y_2O_3:Eu rods exhibited cubic C-type structure, in which XRD peaks fitted to PDF.25–101. According to phase diagram of system Y_2O_3-Eu_2O_3,

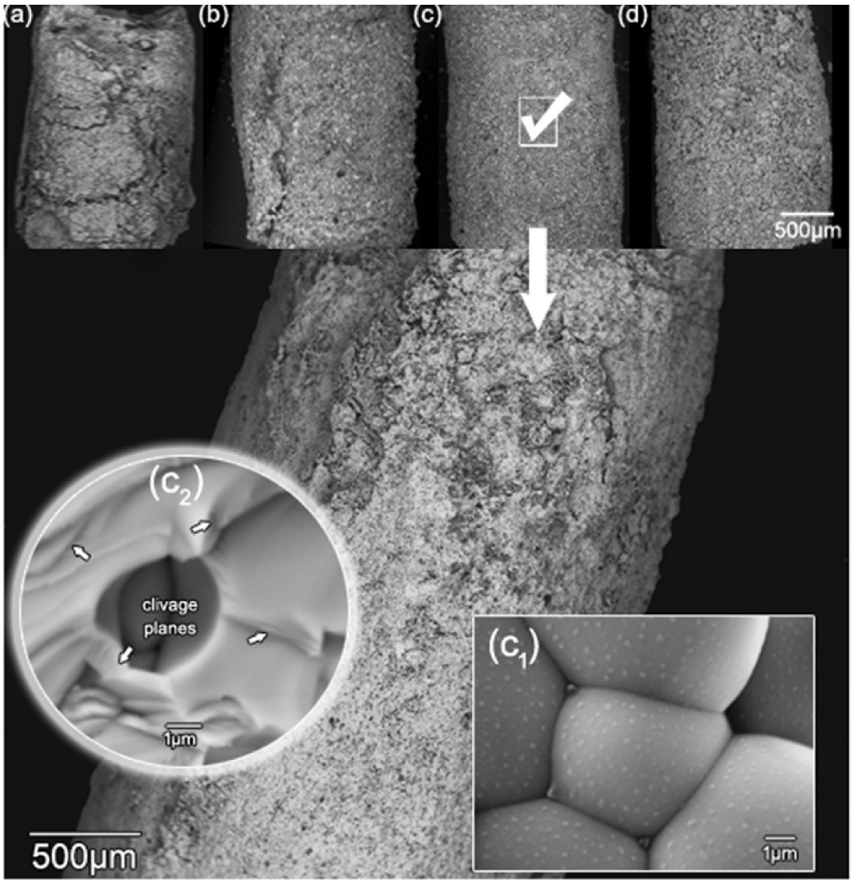

Fig. 9. Development of yttria based rods from replica method. From (a) to (d) morphology and microstructure evolution as a function of sintering parameters. In (c_1) dense surface microstructure and (c_2) fracture microstructure exhibiting cleavage planes.

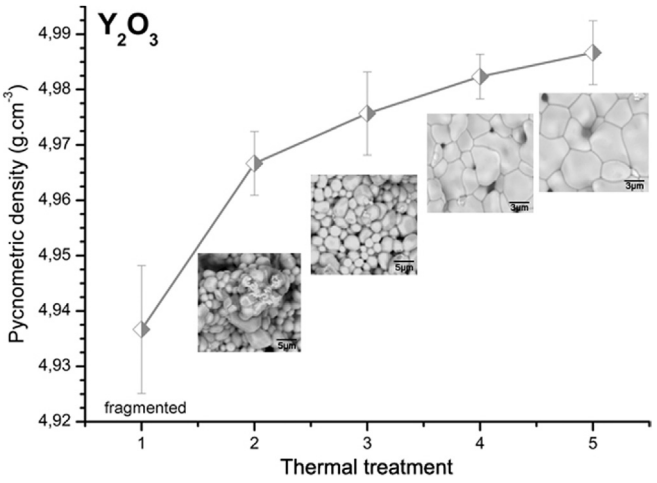

Fig. 10. Density-microstructure evolution of yttria based rods as a function of thermal treatment condition.

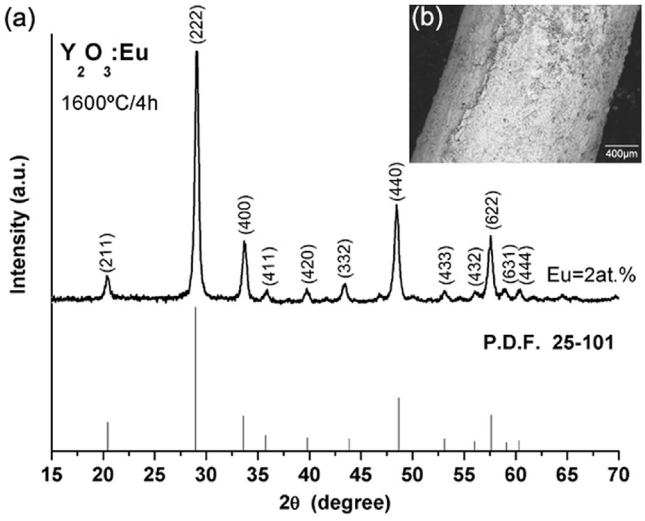

Fig. 11. XRD pattern of as sintered Y_2O_3:Eu rod from sintering condition 4.

cubic C-type structure is the most predominant phase, being stable around of 2200 °C for compositions containing at least 60mol% of Y_2O_3.

The interaction of ionizing radiation with matter leads to development of unpaired electrons, which are detectable by Electron Paramagnetic Resonance (EPR). In addition, rare earths ions (RE) as Eu^{3+}, Tb_{3+}, Dy_{3+}, Yb_{3+} are often incorporated into host structures to the aim of enhance material characteristics as mechanical-chemical strength, thermal stability, and luminescence response. Since Y_2O_3 exhibits intrinsic significant vacancies it is one of the most promising substances for doping with RE ions to develop dosimetric materials. The incorporation of RE ions into Y_2O_3 structure gives rise to rearrangement of its crystal lattice, which provides formation of energy levels and defects. In this way, EPR is a useful technique for characterization of ionizing induced defects, providing substantial information to develop new dosimetric Y_2O_3:Eu based materials.

Fig. 12 illustrates EPR spectra of Y_2O_3:Eu rods as a function of Eu concentration up to 10 at.%. Yttria samples (Eu 0 at.%, narrow line) exhibited two distinct peaks between 345 and 360 mT, where the main peak (c_1) with g value of 2.00 and linewidth around 2.3 mT.

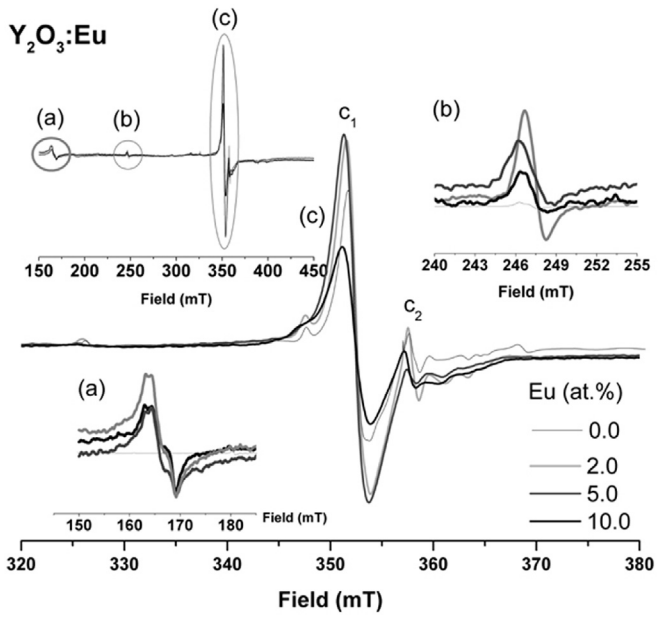

Fig. 12. EPR spectrum of as sintered Y_2O_3:Eu rods as a function of Eu content recorded in room atmosphere.

Lunsford et al. [58] reported that c_1 centre is associated with O^{2-} interstitial íon as a consequence of oxygen adsorption from atmosphere. Osada et al. [51] in their study on Y_2O_3–CaO system observed O^{2-} radical for samples treated in vacuum atmosphere an intense EPR signal with g of around 2.040. On the other hand, for those samples prepared in vacuum no O^{2-} signal was observed. Singh et al. [52] observed the same effect for Y_2O_3:Er samples, in which the main RPE addressed as centre 1 exhibited g of 2.0415. During annealing essays it was observed that centre 1 showed a significant decrease at 160 °C.

The incorporation of europium into yttria host structure led to formation of two new peaks of resonance (a) and (b) which were recorded at 163.5 mT (Fig. 12a) and 248.0 mT (Fig. 12b) with g values of 4.2960 and 2.8540 respectively. The high intense peak c_1 (Fig. 12c) was recorded around 360 mT, with linewidth of 6 mT and g of 2.0040. Considering yttria RPE spectra (thin line), it is seen a displacement of this peak around 0.0040 g. For lower intense peak (c2) the displacement was around 0.0050 g. According to results, it is verified that europium incorporation into yttria host forming news resonance peaks (a-b), intensifies charge carriers and, as a consequence increases EPR response.

Doping Y_2O_3:Eu is performed by replacing Y^{3+} ions for Eu^{3+} ions on sites of yttria lattice, which are C_2 and C_{3i}. The effect of Eu content in promoting EPR response of Y_2O_3:Eu rods considering peak-to-peak height of c_1 centre is illustrated in Fig. 13. The results revealed that the Eu concentration of 5 at.% supplied the most intense peak at g of 1.9970 and linewidth of 4.46 mT. Increasing Eu content towards to 10 at.% leads to decrease EPR signal, in which values are quite similar with those of undoped samples. This effect is ascribed to filling process of symmetry lattice of yttria host, the place in which Eu ions are situated, as well as its concentration. Thus, material characteristics are defined from how RE ion interacts with other ions situated into host material.

Luminescence behavior of phosphors fits well the relation between RE dopant (activator) and host material. In low concentration RE dopant fits symmetry site of host accordingly, transfers its energy to host material as stimulated, rising to intense luminescence. On the other hand, the use of high dopant concentration

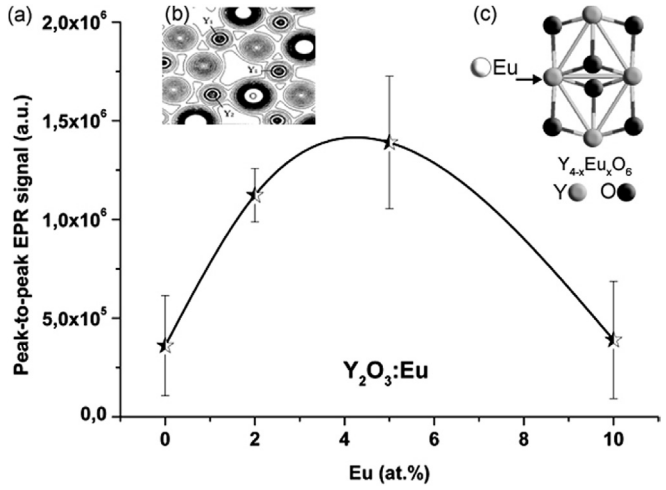

Fig. 13. (a) Effect of Eu doping on promoting paramagnetic defects in yttria host; (b) valence charge density contours in a plane containing Y1–O–Y2 bonding, as reported in Ref. [58]; (c) representation of a crystal cluster from cubic C-type lattice - dark spheres represent oxygen (O) atoms, gray spheres yttrium (Y) atoms and the light sphere means Eu (dopant) atom.

gives rise to decrease the intensity of luminescence due to reduction of space between electronic levels of Eu. Consequently, changes in absorption and emission luminescence spectra as displacement of lines, alterations in intensities, formation of new lines and disappearing of old ones are observed [53].

Govindasamy et al. [54] evaluated theoretically the proprieties of Y_2O_3:Eu using Time-dependent density functional theory (TDDFT). The use of europium as dopant led to formation of samples with wider absorption range, including new absorption bands. Ranson et al. [44]reported that luminescence of yttria is associated with symmetry site in which RE ion is located. Filling of symmetry sites C_{3i}, S_6 result in lower luminescence due to less probability of electronic transitions [55,56]. On the other hand, when RE ions fill C_2 sites, $^5D_0 \rightarrow {}^7F_2$ transitions occur and, consequently provides enhancement of luminescent response [57].

Nian Xu et al. [58] reported a theoretical study on the bond order of Y_2O_3, which means a quantitative measure of the strength of the bond for Y and O in crystal lattice of Y_2O_3. From this study, the chemical bond of Y_2O_3 is far from fully ionic and the bonding between Y and O is significantly covalent. In addition, from the valence charge density maps (Fig. 13c) it is seen that the cubic structure of Y_2O_3 is less closed packed, exhibiting large vacancies at Y and O planes. As a result, these vacancies enable RE ions incorporation and formulation of RE doped yttria based materials (Y_2O_3:RE).

4. Conclusion

Europium-yttria rods (Y_2O_3:Eu) with dimensions of 3.335 mm ± 0.011 mm × 2.271 mm ± 0,014 (height x diameter), weight of 63.701 mg ± 0.021 mg, and electron paramagnetic response were produced by bio-prototyping, in which ceramic powders with mean particle size of 430 nm were synthesized by hydrothermal route at 60 °C for 6 h. Aqueous suspensions with 20 vol% of particles, pH 10, 0.2 wt% of binder exhibited shear thinning behavior and apparent viscosity of 213.00 mPa s. Sintering at 1600 °C for 4 h in air atmosphere provided high densification of ceramic rods with pycnometric density of 4.98 g cm^{-3}, homogeneous microstructure and mechanical strength. Europim-yttria samples exhibited two distinct paramagnetic peaks between 345 and 360 mT, where the main peak with g value of 1.9970 and linewidth around 5.22 mT. The incorporation of europium into yttria host structure led to formation of two new peaks of resonance, which were recorded at 163.5 mT and 248.0 mT with g values of 4.2960 and 2.8540 respectively. The concentration of Eu 5 at.% provided the most intense paramagnetic peak at g of 1.9970 with linewidth of the 4.46 mT due to effective energy transfer from Eu ion to yttria host. These promising results supply substantial processing parameters toward development of new dosimetric materials based on yttria-europium system.

Acknowledgments

We authors are deeply grateful to MSc. Douglas Will Leite and MSc. William Naville from University Centre of FEI. Dr. Sonia Mello and Dr.Chieko Yamagata from IPEN. Besides, Mr. Pedro Garcia from Almatis Brazil. In addition, we thank to São Paulo Research Foundation (FAPESP, grant #2014/23621-3); National Council for Scientific and Technological Development (CNPq); and Coordination for Improvement of High Degree People (CAPES).

References

[1] V.M. Kovrugin, M. Colmont, O.I. Siidra, V.V. Gurzhiy, S.V. Krivovichev, O. Mentre, Pathways for synthesis of new selenium-containing oxo-compounds: chemical vapor transport reactions, hydrothermal techniques and evaporation method, J. Cryst. Growth 457 (2017) 307–313.
[2] V. Fiorenzo, B. John-Christopher, A.C. John, S. Adolfo, B. Marco, A spectroscopic investigation of trivalent lanthanide doped Y 2 O 3 nanocrystals, Nanotechnology 15 (2004) 75.
[3] C. Piccirillo, C.J. Denis, R.C. Pullar, R. Binions, I.P. Parkin, J.A. Darr, P.M.L. Castro, Aerosol assisted chemical vapour deposition of hydroxyapatite-embedded titanium dioxide composite thin films, J. Photochem. Photobiol. A 332 (2017) 45–53.
[4] M. Perez-Page, R. Guzalowski, D.N.F. Muche, R.H.R. Castro, P. Stroeve, Synthesis of porous yttria-stabilized zirconia microspheres by ultrasonic spray pyrolysis, Mater Lett. 188 (2017) 41–44.
[5] B.A.E. Ben-Arfa, I.M.M. Salvado, J.M.F. Ferreira, R.C. Pullar, Novel route for rapid sol-gel synthesis of hydroxyapatite, avoiding ageing and using fast drying with a 50-fold to 200-fold reduction in process time, Mat. Sci. Eng. C-Mater 70 (2017) 796–804.
[6] Q.G. Zhang, T.C. Lu, N. Wei, X.T. Chen, Z.W. Lu, L.J. Chen, J.Q. Qi, Z.Y. Huang, T.F. Hua, S.S. Wang, Y.L. Shi, R.C. Chen, Synthesis of pure-phase uranium-doped YAG powder via co-precipitation method, Mater Lett. 188 (2017) 396–398.
[7] S.H. Jeon, K. Nam, H.J. Yoon, Y.I. Kim, D.W. Cho, Y. Sohn, Hydrothermal synthesis of Nd2O3 nanorods, Ceram. Int. 43 (2017) 1193–1199.
[8] M. Qian, F. Xu, H. Bi, T.Q. Lin, F.Q. Huang, Facile sol-gel method combined with chemical vapor deposition for mesoporous few-layer carbon, Carbon 112 (2017) 47–52.
[9] S.C. Santos, C. Yamagata, A.C. Silva, L.F.G. Setz, S.R.H. Mello-Castanho, Yttrium disilicate micro-cellular architecture from biotemplating of Luffa Cylindrica, J. Ceram. Sci. Technol. 5 (2014) 203–208.
[10] M. Diaz, C. Pecharroman, F. del Monte, J. Sanz, J.E. Iglesias, J.S. Moya, C. Yamagata, S. Mello-Castanho, Synthesis, thermal evolution, and luminescence properties of yttrium disilicate host matrix, Chem. Mater 17 (2005) 1774–1782.
[11] S.C. Santos, J.O. Rodrigues, L.L. Campos, Radiation effects on microstructure and EPR signal of yttrium oxide rods, in: IOP Conference Series: Materials Science and Engineering vol. 169, 2017, p. 012009.
[12] S.C. Santos, W. Acchar, C. Yamagata, S. Mello-Castanho, Yttria nettings by colloidal processing, J. Eur. Ceram. Soc. 34 (2014) 2509–2517.
[13] S.C. Santos, C. Yamagata, W. Acchar, S.R.H.M. Castanho, Yttria nettings by replica processing, Mater. Sci. Forum 798 (2014) 3.
[14] S.C. Santos, C. Yamagata, L.L. Campos, S.R.H. Mello-Castanho, Processing and thermoluminescent response of porous biomorphic dysprosium doped yttrium disilicate burner, Mater Chem. Phys. 177 (2016) 505–511.
[15] S.C. Santos, C. Yamagata, L.L. Campos, S.R.H. Mello-Castanho, Bio-prototyping and thermoluminescence response of cellular rare earth ceramics, J. Eur. Ceram. Soc. 36 (2016) 791–796.
[16] F. Bellaa, A. Chiapponeb, J.R. Naira, G. Meligrana, C. Gerbaldi, Effect of different green cellulosic matrices on the performance of polymeric dye-sensitized solar cells, Chem. Eng. Trans. 41 (2014) 5.
[17] F. Bella, D. Pugliese, L. Zolin, C. Gerbaldi, Paper-based quasi-solid dye-sensitized solar cells, Electrochim Acta 237 (2017) 87–93.
[18] F. Bella, S. Galliano, M. Falco, G. Viscardi, C. Barolo, M. Gratzel, C. Gerbaldi, Approaching truly sustainable solar cells by the use of water and cellulose derivatives, Green Chem. 19 (2017) 1043–1051.

[19] Y. Nishiyama, M. Nakamura, C. Henmi, K. Yamaguchi, S. Mochizuki, H. Nakagawa, K. Takiura, Development of a three-dimensional bioprinter: construction of cell supporting structures using hydrogel and state-of-the-art inkjet technology, J. Biomech. Eng. 131 (2008) 035001–035006.
[20] L. Zolin, J.R. Nair, D. Beneventi, F. Bella, M. Destro, P. Jagdale, I. Cannavaro, A. Tagliaferro, D. Chaussy, F. Geobaldo, C. Gerbaldi, A simple route toward next-gen green energy storage concept by nanofibres-based self-supporting electrodes and a solid polymeric design, Carbon 107 (2016) 811–822.
[21] M. Marina, M.Z.M. Zamzuri, M.N. Derman, M.A. Selamat, Z. Nooraizedfiza, Comparison study in consolidation of yttria reinforced iron-chromium composites using conventional and microwave sintering technique, Adv. Mater. Eng. Technol. Ii 594–595 (2014) 832–836.
[22] F. Hayashi, M. Tanaka, D.M. Lin, M. Iwamoto, Surface structure of yttrium-modified ceria catalysts and reaction pathways from ethanol to propene, J. Catal. 316 (2014) 112–120.
[23] X.M. Han, X. Feng, X.W. Qi, X.Q. Wang, M.Y. Li, The photoluminescent properties of Y2O3:Bi3+, Eu3+, Dy3+ phosphors for white-light-emitting diodes, J. Nanosci. Nanotechnol. 14 (2014) 3387–3390.
[24] A. Jyotsana, G.S. Maurya, A.K. Srivastava, A.K. Rai, B.K. Ghosh, Synthesis and electrical properties of Y2O3: Dy3+ & Eu3+ nanoparticles, Appl. Phys. a-Mater 117 (2014) 1269–1274.
[25] T. Mongstad, A. Thogersen, A. Subrahmanyam, S. Karazhanov, The electronic state of thin films of yttrium, yttrium hydrides and yttrium oxide, Sol. Energ Mat. Sol. C 128 (2014) 270–274.
[26] M.A. Auger, V. de Castro, T. Leguey, J. Tarcisio-Costa, M.A. Monge, A. Munoz, R. Pareja, Effect of yttrium addition on the microstructure and mechanical properties of ODS RAF steels, J. Nucl. Mater 455 (2014) 600–604.
[27] J. Hostasa, J. Matejicek, B. Nait-Ali, D.S. Smith, W. Pabst, L. Esposito, Thermal properties of transparent Yb-Doped yag ceramics at elevated temperatures, J. Am. Ceram. Soc. 97 (2014) 2602–2606.
[28] F.B. Vetrone, J.-C. Capobianco, J.A. Luminescence, Optical Spectroscopy and Applications of Rare Earth Doped Y2O3 Nanocrystals, American Scientific Publishers, Stevenson Ranch, CA, 2003.
[29] L. Zhang, D.Y. Jiang, J.F. Xia, C.X. Li, N. Zhang, Q. Li, Novel luminescent yttrium oxide nanosheets doped with Eu3+ and Tb3+, Rsc Adv. 4 (2014) 17648–17652.
[30] W. Tscharnuter, Photon correlation spectroscopy in particle sizing, in: R.A. Meyers (Ed.), Encyclopedia of Analytical Chemistry, John Wiley & Sons Ltd, 2000, pp. 5549–5585.
[31] A.L. Patterson, The Scherrer formula for x-ray particle size determination, Phys. Rev. 56 (1939) 978–982.
[32] M.L. Nelson, R.T. O'Connor, Relation of certain infrared bands to cellulose crystallinity and crystal lattice type. Part II. A new infrared ratio for estimation of crystallinity in celluloses I and II, J. Appl. Polym. Sci. 8 (1964) 1325–1341.
[33] Q.Z. Duan, Q.H. Yang, S.Z. Lu, C. Jiang, Q. Lu, B. Lu, Fabrication and properties of Er/Tm/Pr tri-doped yttrium lanthanum oxide transparent ceramics, J. Alloy Compd. 612 (2014) 239–242.
[34] C.V. Ramana, V.H. Mudavakkat, K.K. Bharathi, V.V. Atuchin, L.D. Pokrovsky, V.N. Kruchinin, Enhanced optical constants of nanocrystalline yttrium oxide thin films, Appl. Phys. Lett. 98 (2011).
[35] G. Bhavani, S. Ganesan, Structural and optical study of yttrium oxide co-doped with bismuth and zinc prepared by sol-gel method, Indian J. Pure Ap Phys. 54 (2016) 307–312.
[36] Y.C. Liu, Z.W. Hua, Y.R. He, J.Q. Zhu, J.C. Han, Investigation of thermal radiation effect on optical dome of sapphire coated yttrium oxide, Sci. Bull. 61 (2016) 801–810.
[37] M.G. Ivanov, U. Kynast, M. Leznina, Eu3+ doped yttrium oxide nano-luminophores from laser synthesis, J. Lumin 169 (2016) 744–748.
[38] S.S. Li, Y.H. Ji, S.Q. Zhang, S.L. Zhong, C.H. Zeng, Fabrication of Yb3+/Er3+ co-doped yttrium-based coordination polymer hierarchical micro/nano-structures: upconversion luminescence properties and thermal conversion to the corresponding oxides, Crystengcomm 18 (2016) 6809–6816.
[39] A.V. Shevchenko, L.M. Lopato, I.E. Kir'yakova, The reactions of HfO2 with Y2O3, Ho2O3, Er2O3, Tm2 O3, Yb2O3 and Lu2O3 at high temperatures, Izv. Akad. Nauk SSSR Neorg, Mater 20 (1984) 1991–1996.
[40] E.R. Andrievskaya, L.M. Lopato, A.V. Shevchenko, V.P. Smirnov, Phase interaction in the system HfO2–Eu2O3, Izv, RAN Neorg. Mater. 33 (1997) 835–838.
[41] D.V. Tolstikova, M.D. Mikhailov, V.M. Smirnov, Features of the synthesis of nanoparticles of yttrium oxide Y2O3:Nd, Russ. J. Gen. Chem. 84 (2014) 2043–2044.
[42] V. Lojpur, S.P. Ahrenkiel, M.D. Dramicanin, Yb3+, Er3+ doped Y2O3 nanoparticles of different shapes prepared by self-propagating room temperature reaction method, Ceram. Int. 40 (2014) 16033–16039.
[43] L.E. Englade-Franklin, G. Morrison, S.D. Verberne-Sutton, A.L. Francis, J.Y. Chan, J.C. Garno, Surface-directed synthesis of erbium-doped yttrium oxide nanoparticles within organosilane zeptoliter containers, Acs Appl. Mater Inter 6 (2014) 15942–15949.
[44] R.M. Ranson, E. Evangelou, C.B. Thomas, Modeling the fluorescent lifetime of Y2O3 : Eu, Appl. Phys. Lett. 72 (1998) 2663–2664.
[45] A.T. Hutton, R.M. Hartshorn, N.G. Connelly, T. Damhus, Nomenclature of Inorganic Chemistry, RSC Publishing, 2005.
[46] X.-M. Zhang, M.-L. Huang, Z.-J. Zhang, B.-Q. Liu, J.-T. Zhao, Daisy-like Y(OH)3: Eu/Y2O3:Eu microstructure: formation and luminescence properties, Mater Lett. 68 (2012) 269–272.
[47] N.J. Shivaramu, B.N. Lakshminarasappa, K.R. Nagabhushana, F. Singh, Synthesis characterization and luminescence studies of gamma irradiated nanocrystalline yttrium oxide, Spectrochim. Acta A 154 (2016) 220–231.
[48] B.A. Prakasam, M. Lahtinen, A. Peuronen, M. Muruganandham, M. Sillanpaa, Facile fabrication of flower like self-assembled mesoporous hierarchical microarchitectures of In(OH)(3) and In2O3: in(OH)(3) micro flowers with electron beam sensitive thin petals, Mater Chem. Phys. 184 (2016) 183–188.
[49] R. Moreno, Reología de suspensiones cerámicas, Consejo Superior de Investigaciones Científicas, Madrid, 2005.
[50] J. Mewis, N.J. Wagner, Thixotropy, Adv. Colloid Interfac. 147–48 (2009) 214–227.
[51] O.M. Bordun, Influence of oxygen vacancies on the luminescence spectra of Y2O3 thin films, J. Appl. Spectrosc. 69 (2002) 430–433.
[52] V. Singh, V.K. Rai, I. Ledoux-Rak, S. Watanabe, T.K.G. Rao, J.F.D. Chubaci, L. Badie, F. Pelle, S. Ivanova, NIR to visible up-conversion, infrared luminescence, thermoluminescence and defect centres in Y(2)O(3) : Er phosphor, J. Phys. D. Appl. Phys. 42 (2009).
[53] A. Tannhäuser, Über die Wechselwirkung äquivalenter Erbium-Ionen in kristallinem (Er, Y)2O3, Z Phys. 170 (1962) 533–539.
[54] A. Govindasamy, C. Lv, H. Tsuboi, M. Koyama, A. Endou, M. Kubo, E. Broclawik, A. Miyamoto, A theoretical study of the effect of Eu ion dopant on the electronic excitations of yttrium oxide and yttrium oxy-sulphide, Jpn. J. Appl. Phys. 1 (45) (2006) 5782–5785.
[55] H. Forest, G. Ban, Evidence for Eu+3-Emission from 2 symmetry sites in Y2o3-Eu+3, J. Electrochem Soc. 116 (1969), 474-&.
[56] E. Zych, M. Karbowiak, K. Domagala, S. Hubert, Analysis of Eu3+ emission from different sites in Lu2O3, J. Alloy Compd. 341 (2002) 381–384.
[57] A. Konrad, T. Fries, A. Gahn, F. Kummer, U. Herr, R. Tidecks, K. Samwer, Chemical vapor synthesis and luminescence properties of nanocrystalline cubic Y2O3 : Eu, J. Appl. Phys. 86 (1999) 3129–3133.
[58] Y.N. Xu, Z.Q. Gu, W.Y. Ching, Electronic, structural, and optical properties of crystalline yttria, Phys. Rev. B 56 (1997) 14993–15000.